Heliyon

Received:
27 November 2018
Revised:
4 March 2019
Accepted:
25 March 2019

Cite as: Anh Thi Le, Swee-Yong Pung, Srimala Sreekantan, Atsunori Matsuda, Dai Phu Huynh. Mechanisms of removal of heavy metal ions by ZnO particles. Heliyon 5 (2019) e01440. doi: 10.1016/j.heliyon.2019.e01440

Mechanisms of removal of heavy metal ions by ZnO particles

Anh Thi Le [a], Swee-Yong Pung [a,*], Srimala Sreekantan [a], Atsunori Matsuda [b], Dai Phu Huynh [c]

[a] *School of Materials and Mineral Resources Engineering, Universiti Sains Malaysia Engineering Campus, Nibong Tebal, Pulau Pinang, Malaysia*

[b] *Department of Electrical and Electronic Information Engineering, Toyohashi University of Technology, Toyohashi, Aichi, Japan*

[c] *Faculty of Materials Technology, National Key Lab. of Polymer and Composite Materials, Ho Chi Minh University of Technology, Vietnam National University, Ho Chi Minh City, Viet Nam*

[*] Corresponding author.
E-mail address: sypung@usm.my (S.-Y. Pung).

Abstract

Effluent discharges from industry and domestic waste containing unknown inorganic pollutants. In this work, different mechanisms of heavy metal ions removal using ZnO particles were studied. ZnO particles were synthesized using solid precipitation technique. The morphology of ZnO particles was rod-like shape. The average length and diameter of ZnO particle were 497.34 ± 15.55 and 75.78 ± 10.39nm, respectively. These particles removed effectively heavy metal ions such as Cu(II), Ag(I) and Pb(II) ions with efficiency >85% under exposure of 1 hour of UV light. However, poor removal efficiency, i.e. <15% was observed for Cr(VI), Mn(II), Cd(II) and Ni(II) ions. The removal of these heavy metal ions was in the forms of metals or metal oxide via reduction/oxidation or adsorption mechanism.

Keywords: Materials science, Nanotechnology

https://doi.org/10.1016/j.heliyon.2019.e01440

1. Introduction

Water pollution is one of the consequences of rapid development of industry and expansion of human population. Thus, this leads to exhausting of fresh water resources. Dumping of untreated industrial and domestic waste containing inorganic compounds in water bodies causes water-borne diseases. In addition, long-term excessive ingestion of these pollutants particularly heavy metal ions such as Chromium (Cr), Copper (Cu), Manganese (Mn), Nickel (Ni), Lead (Pb), Silver (Ag) and Cadmium (Cd) could damage kidney, liver, brain function, nervous system or even death. Various treatment techniques have been developed for the removal of inorganic and organic contaminants from wastewater such as chemical treatment [1, 2], filtration [3, 4], ion exchange [5] and absorption [6, 7] techniques. However, these techniques do not eliminate the contaminants completely. Advanced oxidation process using heterogeneous photocatalysts such as titanium dioxide (TiO_2) [8, 9, 10] and zinc oxide (ZnO) [11, 12, 13] is another alternative technique which is extensively studied by researchers as it can remove both inorganic and organic contaminants simultaneously.

In this work, ZnO particles was chosen because it is cheap and has good photocatalytic performance in heavy metal ions removal [14, 15]. The high surface area of ZnO particles is responsible for adsorbing positive metal ions in the wastewater effectively [14, 16]. Most researches have been focused on the reduction of toxic Cr(VI) by using ZnO photocatalyst [17, 18, 19, 20, 21, 22]. A limited study was carried out to remove other metal ions such as Ag(I), Mn(II), Cd(II), Ni(II) [23], Cu(II) [24] and Pb(II) [25] ions by ZnO photocatalyst. Wang et. al. [16] reported that the ZnO hollow microspheres enhanced the removal of Cu(II), Cd(II) and Pb(II) cations compared with the commercial ZnO particles. Nonetheless, no comparison study on the removal of metal ions i.e. Cu(II), Ag(I), Pb(II), Cr(VI), Mn(II), Cd(II), and Ni(II) ions by ZnO was performed under the same testing condition. Furthermore, the heavy metal ions removal mechanism might be more complicated than the common accepted idea, i.e. via reduction of cations [26]. The heavy metal ions mechanism(s) could be varied depends on the types of metal ions and light sources. In this paper, the capabilities of ZnO particles in removal of Cu(II), Ag(I), Pb(II), Cr(VI), Mn(II), Cd(II), and Ni(II) ions in aqueous solution under UV light and visible light condition was assessed. In addition, based on the analysis of the end products, the removal mechanisms of each metal ions by ZnO particles were deduced.

2. Materials and methods

2.1. Materials

Zinc nitrate tetrahydrate ($Zn(NO_3)_2.4H_2O$, Merck, 108833), hexamethylenetetramine ($C_6H_{12}N_4$, Merck, 818712) and polyvinylpyrrolidone ($(C_6H_9NO)_n$,

https://doi.org/10.1016/j.heliyon.2019.e01440

Sigma-Aldrich, 81440) were used to synthesize ZnO particles. Heavy metal sources were nickel nitrate hexahydrate ($Ni(NO_3)_2$, Merck, 106721), lead nitrate ($Pb(NO_3)_2$, Fluka, 15335), copper sulfate ($CuSO_4$, Merck, 102791), silver nitrate ($AgNO_3$, Qrel, 55152), potassium dichromate ($K_2Cr_2O_7$, C&L, 488), manganese (II) acetate tetrahydrate ($(CH_3COO)_2Mn.4H_2O$, Merck, 843487), cadmium acetate ($C_4H_{10}CdO_6$, Fisher, C4-500).

2.2. Preparation of ZnO photocatalyst

The synthesis of ZnO particles followed the procedure as described by Thein et al. [11]. In this process, 3.1g zinc nitrate tetrahydrate, 1.7g hexamethylenetetramine and 0.4g of polyvinylpyrrolidone were dissolved in 100ml distilled water. The zinc nitrate tetrahydrate and hexamethylenetetramine solution were added into polyvinylpyrrolidone solution. The mixture was stirred 60 min at room temperature. The temperature of water bath was set at 90 °C for 45min for the growth of ZnO particles. The ZnO particles were collected by centrifugation. The particles were washed several times with distilled water before drying in the oven at 100 °C.

2.3. Removal of heavy metal ions

The UV and visible light was used to trigger the photocatalytic reaction in removal of heavy metal ions such as Cu(II), Pb(II), Ag(I), Cr(VI), Cd(II), Mn(II), Ni(II) by ZnO particles. In each tests, 50ppm of single-element solution was added with ZnO particles (1 g/l) and stirred magnetically in the dark for 30min for adsorption/desorption equilibrium. The light source was then turned on for the photocatalytic reaction. These heavy metal ions were removed from solution by depositing onto the surface of ZnO particles, resulting formation of metal/metal oxide coupled ZnO hybrid particles. Then, the concentrations of heavy metal ions in solution were measured in every 15min time interval using Inductive Couple Plasma – Optical Emission Spectrometry (ICP-OES). The heavy metal ions removal efficiency (η) of ZnO particles was calculated using Eq. (1),

$$\eta(\%) = \left(\frac{C_o - C_t}{C_o}\right)100 \tag{1}$$

where C_o and C_t were the concentration of metal ions at the initial and time t, respectively.

These hybrid particles were collected by centrifugation and dried at 100 °C for 8hr. For the ease of identification, the hybrid particles collected after heavy metal/metal oxide deposition were designated as M/ZnO particles, where M was referred to the metal ions used in the study, i.e. Cu, Pb, Ag, Cr, Cd, Mn, and Ni.

https://doi.org/10.1016/j.heliyon.2019.e01440

2.4. Characterizations

The crystal structure of ZnO particles and M/ZnO were characterized by X-ray Diffractometer (XRD, Bruker D8- Discovery) with a copper-monochrome Cu-K radiation source ($K_\alpha = 1.54056$ Å) scanning from 10° to 90°. Joint Committee on Powder Diffraction Standards (JCPDS) database was used as a reference to match the XRD spectrum. The chemical states of heavy metal ions after deposition were analysed by X-ray Photoelectron Spectrometer (Axis Ultra DLD - XPS, Kratos). XPS data was analysed using CasaXPS software. The carbonaceous (C 1s) was used as a reference to calibrate the binding energies. The High Resolution Transmission Electron Microscope (HRTEM) image was obtained by Tecnai G220 S-Twin. Elemental distribution of metal on ZnO was performed by using an Energy Dispersive X-ray (EDX) mapping analysis.

3. Results and discussion

3.1. Heavy metal ions removal by ZnO particles

Fig. 1(a), (b) show the removal efficiency of heavy metal ions by ZnO particles under visible light and UV light, respectively. Generally, ZnO particles were able to remove heavy metal ions with different efficiencies after 1 hour irradiation under

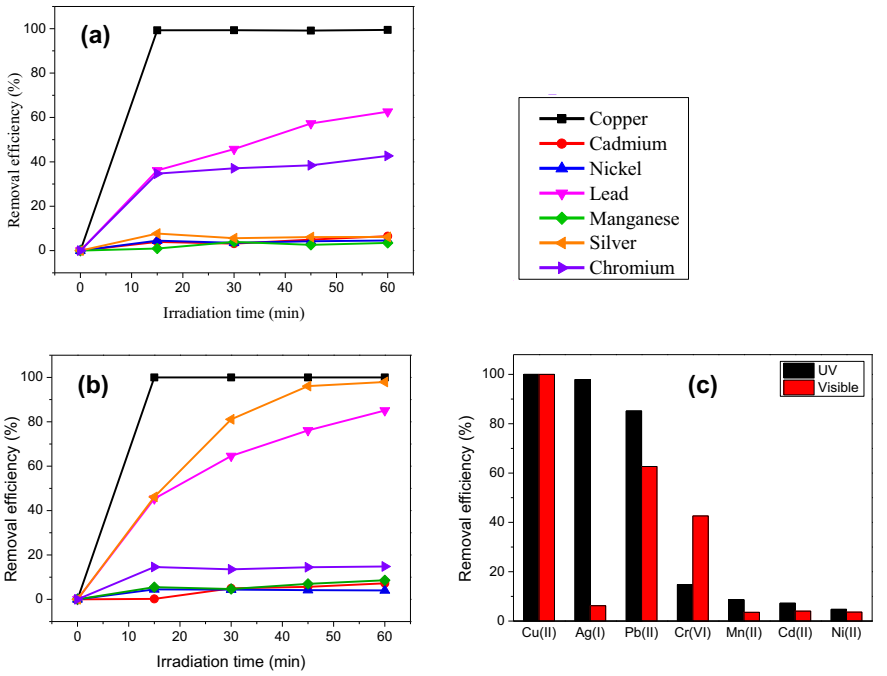

Fig. 1. The removal efficiency of Cu, Ag, Pb, Cr, Mn, Cd and Ni ions in the aqueous solution of ZnO particles under (a) visible light irradiation, (b) UV light irradiation and (c) removal efficiency of heavy metal ions after 1 hour irradiation of visible light and UV.

https://doi.org/10.1016/j.heliyon.2019.e01440

different light sources as depicted in Fig. 1(c). A few hypotheses on the removal mechanisms of metal ions by ZnO particles could be drawn by comparing the observation in Fig. 1.

(i) Not responsive to the type of light sources (optical excitation source)

ZnO particles demonstrated excellent removal efficiency i.e. 100.00% for Cu(II) ions whereas poor removal efficiency i.e. $< 9.00\%$ for Mn(II), Cd(II) and Ni(II) ions, regardless the types of light sources. As the energy of visible light was insufficient for ZnO particles to produce electrons/holes for photo-reduction/photo-oxidation, the removal of these metal ions by ZnO particles suggests that it was due to physical absorption process.

(ii) Responsive to the type of light sources (optical excitation source)

ZnO particles removed a small amount of Ag(I) ions under visible light. However, it achieved 97.92% removal efficiency under UV exposure. This observation suggests that the removal of Ag(I) ions by ZnO particles was via photocatalytic reduction. Similarly, ZnO particles were able to remove Pb(II) ions moderately via physical adsorption under visible light with removal efficiency $\sim 62.65\%$. Nevertheless, the removal efficiency increased to 85.18% under UV irradiation. This result suggests that the removal mechanism could be a mixture of physical adsorption and photocatalytic reduction under UV light. It is noted that ZnO particles displayed moderate efficiency of $\sim 43.34\%$ to remove Cr(VI) ions from solution via physical adsorption under visible light. Interestingly, the removal efficiency reduced drastically to 14.83% under UV exposure. The removal mechanism of Cr(VI) ions by ZnO particles is discussed in subsection 3.3 after more evident were collected in subsequent analysis. Based on these results, the possible removal mechanisms of heavy metal ions are summarized in Table 1.

Table 1. Heavy metal ion removal efficiency and possible removal mechanism of heavy metal ions removal by ZnO particles.

Heavy metal ions	Removal efficiency			Possible removal mechanism
	Visible/dark	UV	Trend	
Ag (I)	Poor	Good	↑	A + R/O
Cr (VI)	Moderate	Poor	↓	A + R/O
Pb (II)	Moderate	Good	↑	A + R/O
Mn (II)	Poor	Poor	No significant change	A
Cu (II)	Good	Good	No significant change	A
Cd (II)	Poor	Poor	No significant change	A
Ni (II)	Poor	Poor	No significant change	A

Legends: Adsorption − A, Reduction − R, Oxidation − O.

https://doi.org/10.1016/j.heliyon.2019.e01440

3.2. Structural properties of M/ZnO hybrid particles

Figs. 2(a) and 3(a) show the XRD patterns of ZnO particles and M/ZnO hybrid particles collected after heavy metal ions removal under visible light and UV light irradiation, respectively. Generally, the diffraction peaks at 31.09°, 33.77°, 35.56°, 46.89°, 55.96°, 62.27°, 65.79°, 67.38°, 68.51°, 76.41° and 89.09° are corresponded to (100), (002), (101), (102), (110), (103) and (112) crystal planes of hexagonal ZnO structures (JCPDS No. 98-002-7791), respectively. According to the reference, the lattice constant of ZnO are a = 3.25nm and c = 5.21nm. Besides diffraction peaks related to ZnO, additional diffraction peaks could be identified in each of M/ZnO hybrid particles.

For instance, the XRD patterns of Cu/ZnO hybrid particles are displayed in Figs. 2(b) and 3(b). The CuO phase was detected with additional planes of (002), (020) and (202) at diffraction peaks of 35.6°, 56.3° and 61.1° in both UV and visible light irradiation. The diffraction peaks of CuO were indexed to the monoclinic CuO crystal phase (JCPDS card No.: 98-005-9312).

Only diffraction peaks belong to ZnO were measured for Ag/ZnO hybrid particles collected after visible light irradiation as shown in Fig. 2(c). In contrary, under UV process, the Ag/ZnO hybrid particles shown additional planes of (111), (112)

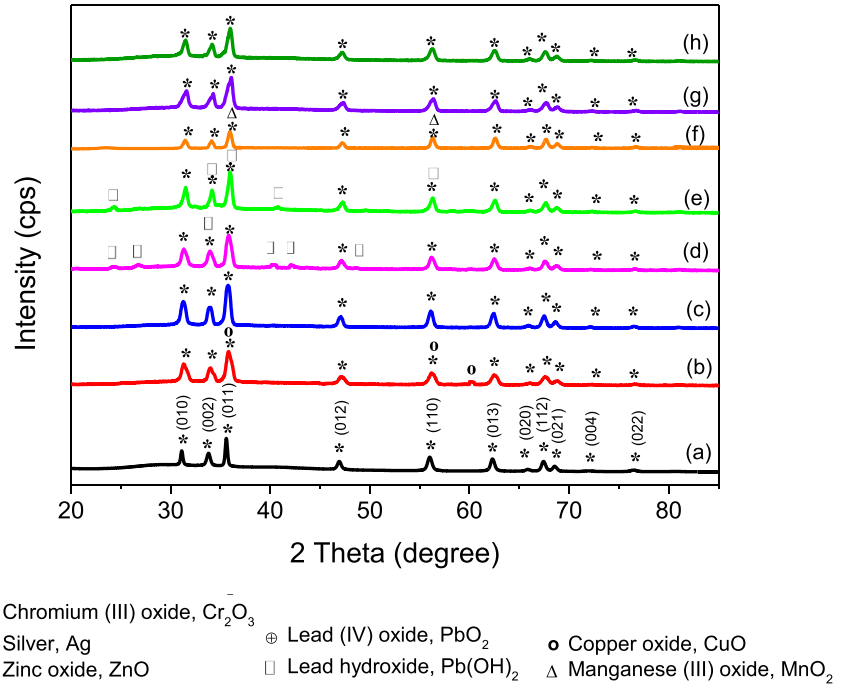

Fig. 2. XRD spectra of (a) ZnO particles, (b) Cu/ZnO, (c) Ag/ZnO, (d) Pb/ZnO, (e) Cr/ZnO, (f) Mn/ZnO, (g) Cd/ZnO and (h) Ni/ZnO hybrid particles. The deposition of heavy metals were carried out under visible light irradiation.

https://doi.org/10.1016/j.heliyon.2019.e01440

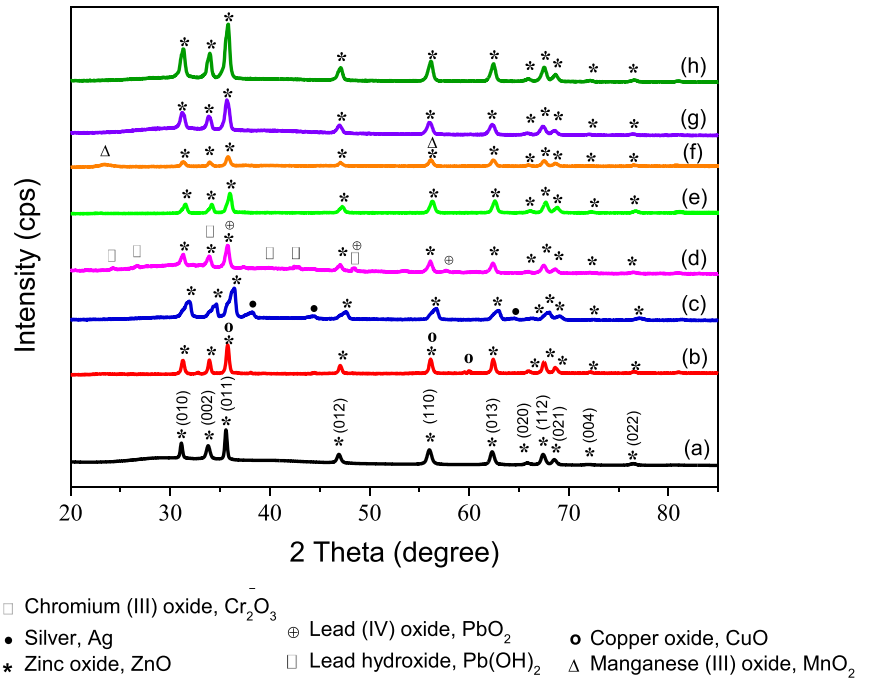

Fig. 3. XRD spectra of (a) ZnO particles, (b) Cu/ZnO, (c) Ag/ZnO, (d) Pb/ZnO, (e) Cr/ZnO, (f) Mn/ZnO, (g) Cd/ZnO and (h) Ni/ZnO hybrid particles. The deposition of heavy metals were carried out under UV light irradiation.

and (222) at diffraction peaks of 38.29°, 44.49° and 64.52°, corresponding to silver cubic structure (JCPDS card No.: 98-008-3900) as shown in Fig. 3(c). The result suggests that the deposition of Ag, if there was any, was below the detection limit of XRD.

Figs. 2(d) and 3(d) depict the XRD pattern of Pb/ZnO hybrid particles collected from the visible/ZnO and UV/ZnO processes, respectively. The $Pb(OH)_2$ phase was detected in both Pb/ZnO hybrid particles from both UV and visible processes. The diffraction peaks of $Pb(OH)_2$ appeared in 24.5°, 26.7°, 34.3°, 40.0°, 43.7 ° and 48.6°, corresponding to (102), (103), (110), (210), (203) and (204) crystal planes, respectively. The structure of $Pb(OH)_2$ precipitate was hexagonal with a = 5.3Å, c = 12.8 Å, c/a = 2.4. Fig. 3(d) depicted the addition peaks of PbO_2 in the Pb/ZnO hybrid particles, indicating oxidation of Pb(II) ions under irradiation of UV light. The XRD peaks of PbO_2 were observed at 35.8°, 48.6° and 60.1°, which match with the JCPDS card No.: 98-001-7317 of PbO_2 tetragonal structure.

The presence of Cr_2O_3 phase on the XRD peaks of Cr/ZnO hybrid particles collected from visible illumination process was observed in Fig. 2(e). Additional diffraction peaks of Cr_2O_3 phase were found at 24.3°, 34.2°, 35.9°, 40.7° and 56.2°, corresponding to (012), (104), (110), (006) and (116) plane. The Cr_2O_3 phase was indexed to the JCPDS card No.: 98-011-4621 of hexagonal structure. The quantity of ZnO and Cr_2O_3 crystal phase were 74% and 26%, respectively as measured using PAN

https://doi.org/10.1016/j.heliyon.2019.e01440

analytical X"pert High Score Plus software. However, no extra diffraction peaks could be seen from the Cr/ZnO hybrid particles by UV light irradiation as presented in Fig. 3(e).

Figs. 2(f) and 3(f) present the diffraction pattern of Mn/ZnO hybrid particles obtained from the photocatalytic reaction under visible and UV irradiation, respectively. In Fig. 2(f), no other crystal phases except ZnO could be found on Mn/ZnO hybrid particles after visible irradiation. Nevertheless, additional peaks at 23.5° and 56.3° were found to be the MnO_2 cubic structure of JCPDS card No.: 98-005-1771 under UV exposure as shown in Fig. 3(f).

The crystal structure of Cd/ZnO hybrid particles was characterized via X-ray diffraction as seen in Figs. 2(g) and 3(g). There was no change in crystal structure of Cd/ZnO hybrid particles as compared to ZnO particles, suggesting that the Cd or CdO, if there was any, presented in a very low concentration on the surface of ZnO particles. Similarly, no additional XRD peak was found on Ni/ZnO hybrid particles as shown in Figs. 2(h) and 3(h). This result agrees well with the result shown in Fig. 1(c) as ZnO particles exhibited poor removal efficiency for both Cd(II) and Ni(II) ions.

The formation of metals or metal oxides onto ZnO particles after the removal of metal ions under UV light irradiation was further evaluated using XPS analysis. As shown in Fig. 4(a), the element of zinc (Zn), oxygen (O), Cu, and carbon (C) were observed. The high peak of Zn 2p and O 1s exhibited the high content of Zn

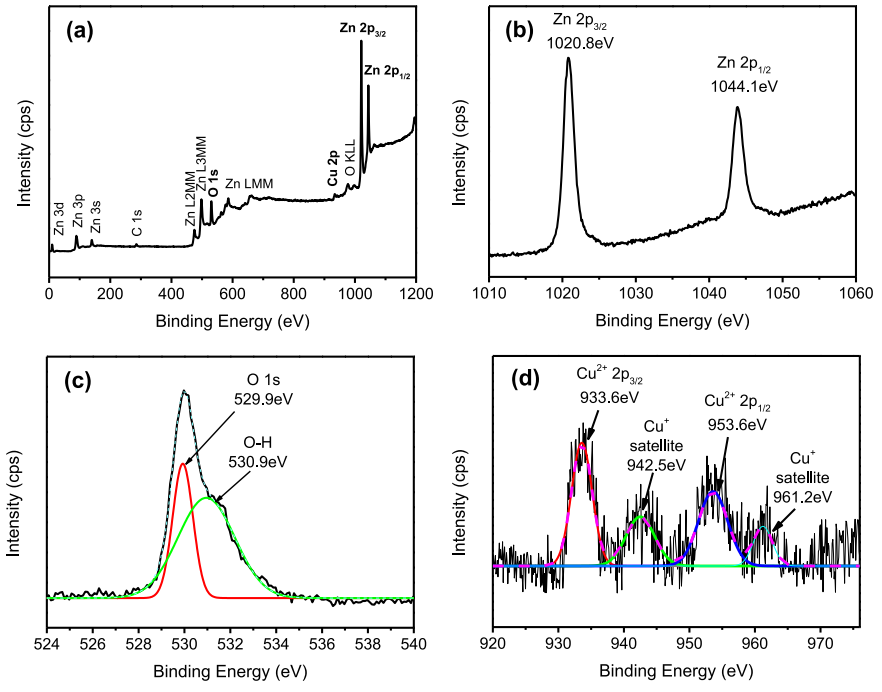

Fig. 4. XPS spectra of Cu/ZnO hybrid particles. (a) Wide scan and high-resolution scan of (b) Zn 2p, (c) O 1s, and (d) Cu 2p state energies.

https://doi.org/10.1016/j.heliyon.2019.e01440

and O elements as compared to Cu and C elements. The presence of C 1s peak at 284.6eV of binding energy was due to the surface adventitious carbon. Fig. 4(b) shows the high-resolution of Zn $2p_{3/2}$ and Zn $2p_{1/2}$ corresponded to the binding energy of 1020.8eV and 1044.1eV of ZnO, respectively. The high-resolution O 1s spectrum was depicted in Fig. 4(c). It could be de-convoluted into two peaks at 529.9eV and 530.9eV, which assigned to O^{2-} of ZnO or CuO and the absorbed water, respectively. In Fig. 4(d), the two Cu 2p peaks are located at 933.6eV and 953.6eV. The gap between Cu $2p_{3/2}$ and Cu $2p_{1/2}$ is around 20eV, which is in agreement with CuO standard spectrum [27]. The presence of Cu shakeup satellite peaks at 942.5eV and 961.2eV could be attributed by Cu_2O phase. Similar finding was reported by Munawar et al. [28].

The whole survey of the XPS spectra (Fig. 5(a)) indicate the presence of Zn, O, and Ag elements in the Ag/ZnO hybrid particles. Fig. 5(b) shows the high-resolution scan of Ag $3d_{5/2}$ and Ag $3d_{3/2}$ fitted well with the metallic Ag^0 oxidation state at 368.4eV and 375.2eV of binding energy [29]. The results are in agreement with the XRD as previously discussed, which highlight the deposition of Ag particles onto the ZnO particles. Fig. 6(a) shows the presence of Zn, O, and Pb elements in Pb/ZnO hybrid particles as expected. The high-resolution of Pb 4f spectrum (Fig. 6(b)) exhibited two main peaks at 138.0eV and 142.8eV, that could be assigned to binding energy of Pb $4f_{7/2}$ and Pb $4f_{3/2}$ of PbO_2, respectively [30, 31]. Furthermore, the peak centred at 139.0eV corresponds to the Pb^{2+} cation associated with $Pb(OH)_2$ or PbO formation. The XPS survey scan spectrum (Fig. 7(a)) demonstrates that the Cr/ZnO hybrid particles was mainly composed of Zn, O, and Cr elements. As shown in Fig. 7(b), the Cr 2p XPS spectrum shows two split spin orbitals at 576.6eV for Cr $2p_{3/2}$ and 585.4eV for Cr $2p_{1/2}$ corresponding to the Cr^{3+} oxidation state [32]. As demonstrated in Fig. 8(a), the XPS spectra of Mn/ZnO hybrid particles show the peaks associated with Zn, O, and Mn elements. The binding energies of Mn $2p_{3/2}$ and Mn $2p_{1/2}$ were located at 641.5eV and 658.8eV, respectively, as shown in Fig. 8(b), which is in good agreement with binding energy reference of MnO_2 [33]. In contrary, Fig. 9 (a) exhibits XPS signal of Ni/ZnO hybrid particles, which presents

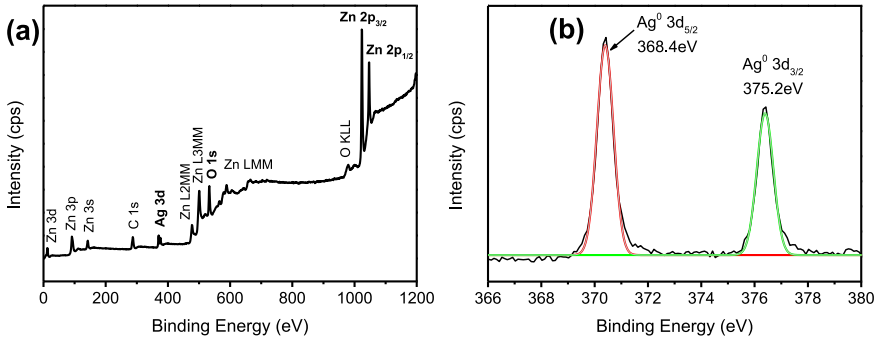

Fig. 5. XPS spectra of Ag/ZnO hybrid particles. (a) Wide scan, and (b) high-resolution scan.

https://doi.org/10.1016/j.heliyon.2019.e01440

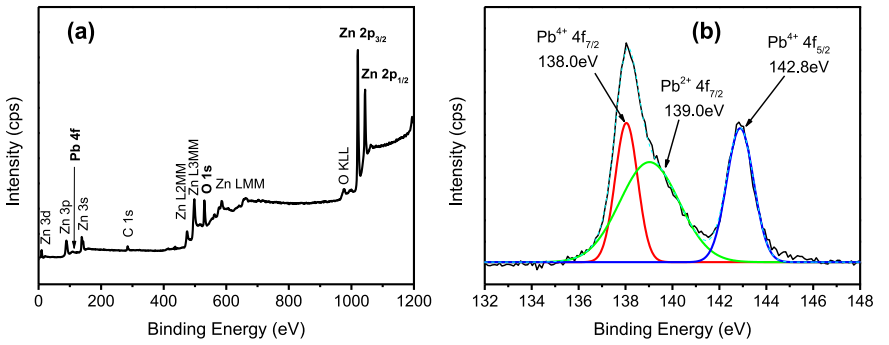

Fig. 6. XPS spectra of Pb/ZnO hybrid particles. (a) Wide scan, and (b) high-resolution scan.

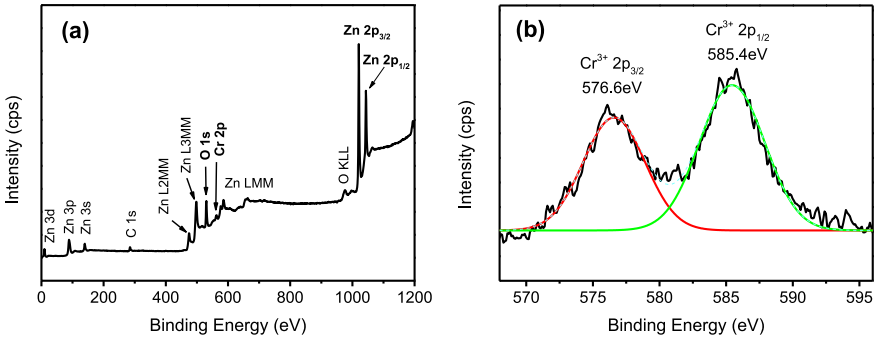

Fig. 7. XPS spectra of Cr/ZnO hybrid particles. (a) Wide scan, and (b) high-resolution scan.

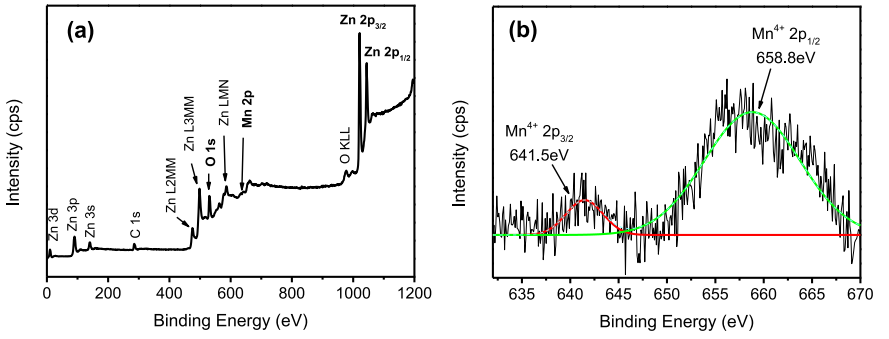

Fig. 8. XPS spectra of Mn/ZnO hybrid particles. (a) Wide scan, and (b) high-resolution scan.

only the elements of Zn and O. The Ni 2p binding energy was not detected by high-resolution XPS as depicted in Fig. 9(b). This is due to the low removal efficiency of Ni(II) ion from the solution, which is consistent with the XRD results. The XPS analysis of Cd/ZnO hybrid particles was not carried out due to its poor removal efficiency by ZnO particles.

Fig. 10(a) shows that the ZnO particles were rod-like shape. The average length and diameter of ZnO particles were 497.34 $\pm$ 15.55nm and 75.78 $\pm$ 10.39nm, respectively. The morphology of Cu/ZnO hybrid particles was shown in Fig. 10(b). The

https://doi.org/10.1016/j.heliyon.2019.e01440

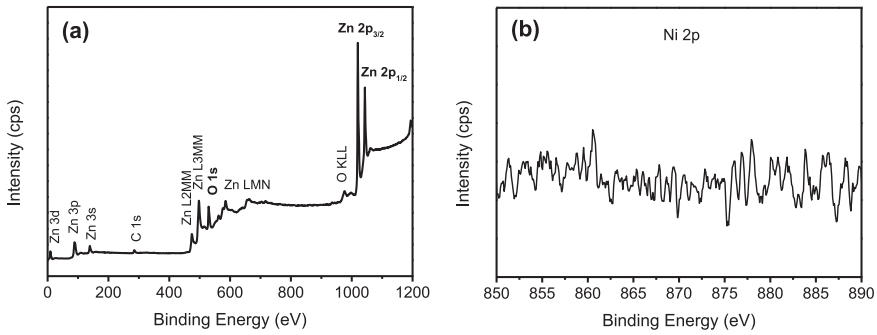

Fig. 9. XPS spectra of Ni/ZnO hybrid particles. (a) Wide scan, and (b) high-resolution scan.

ZnO particles have rough surface with increasing diameter and length, i.e. 105.11 ± 13.76nm and 627.22 ± 16.69nm, respectively. Fig. 10(c) presents the ZnO particles that have smooth surface after removal of Ag under visible light. The average diameter and length of Ag/ZnO hybrid particles were 76.67 ± 15.43nm and 520.49 ± 17.82nm, respectively. It is noted that plate-like structures were observed in Pb/ZnO hybrid particles as displayed in Fig. 10(d). The average diameter and length of ZnO particles in Pb/ZnO hybrid particles were 95.56 ± 16.18nm and 520.32 ± 14.86nm, respectively. As seen in Fig. 10(e), some plate-like structures could also be found although no obvious tiny particles on the surface of Cr/ZnO hybrid particles in the use of visible light. The colour of Cr/ZnO hybrid particles collected was yellowish. The average diameter and length of Cr/ZnO hybrid particles were 104.99 ± 12.52nm and 519.95 ± 13.05nm, respectively. Fig. 10(f) shows the morphology of Mn/ZnO hybrid particles with the presence of some tiny particles on its surface. The average diameter and length of Mn/ZnO hybrid particles were 94.37 ± 10.60nm and 566.82 ± 15.65nm, respectively. No foreign particles and significant increase in particles size could be observed for Cd/ZnO hybrid particles and Ni/ZnO hybrid particles as shown in Fig. 10(g) and (h), respectively. The average diameter and length of Cd/ZnO hybrid particles were 94.46 ± 11.36nm and 583.73 ± 18.59nm, respectively. The average diameter and length of Ni/ZnO hybrid particles were 96.43 ± 12.79nm and 561.35 ± 15.53nm, respectively. This was attributed to their poor removal efficiency for Cd(II) and Ni(II) ions as shown in Fig. 1(c).

Fig. 11 shows the morphology of ZnO hybrid particles collected after heavy metal ions removal under UV light. As displayed in Fig. 11(a), the surface of Cu/ZnO hybrid particles was coated with a rough layer. The average length and diameter of Cu/ZnO hybrid particles were 764.35 ± 11.39nm and 145.49 ± 10.02nm, respectively. The significant increase of particle size suggests the deposition of Cu(II) ions on ZnO particles. Fig. 11(b) shows the SEM image Ag/ZnO hybrid particles after the UV irradiation process. The average length of Ag/ZnO hybrid particles was 577.21 ± 13.53nm, whereas the average diameter was 102.28 ± 12.54nm. It is noted that tiny particles (marked in red cycles) with diameter <20nm were found on the surface

https://doi.org/10.1016/j.heliyon.2019.e01440

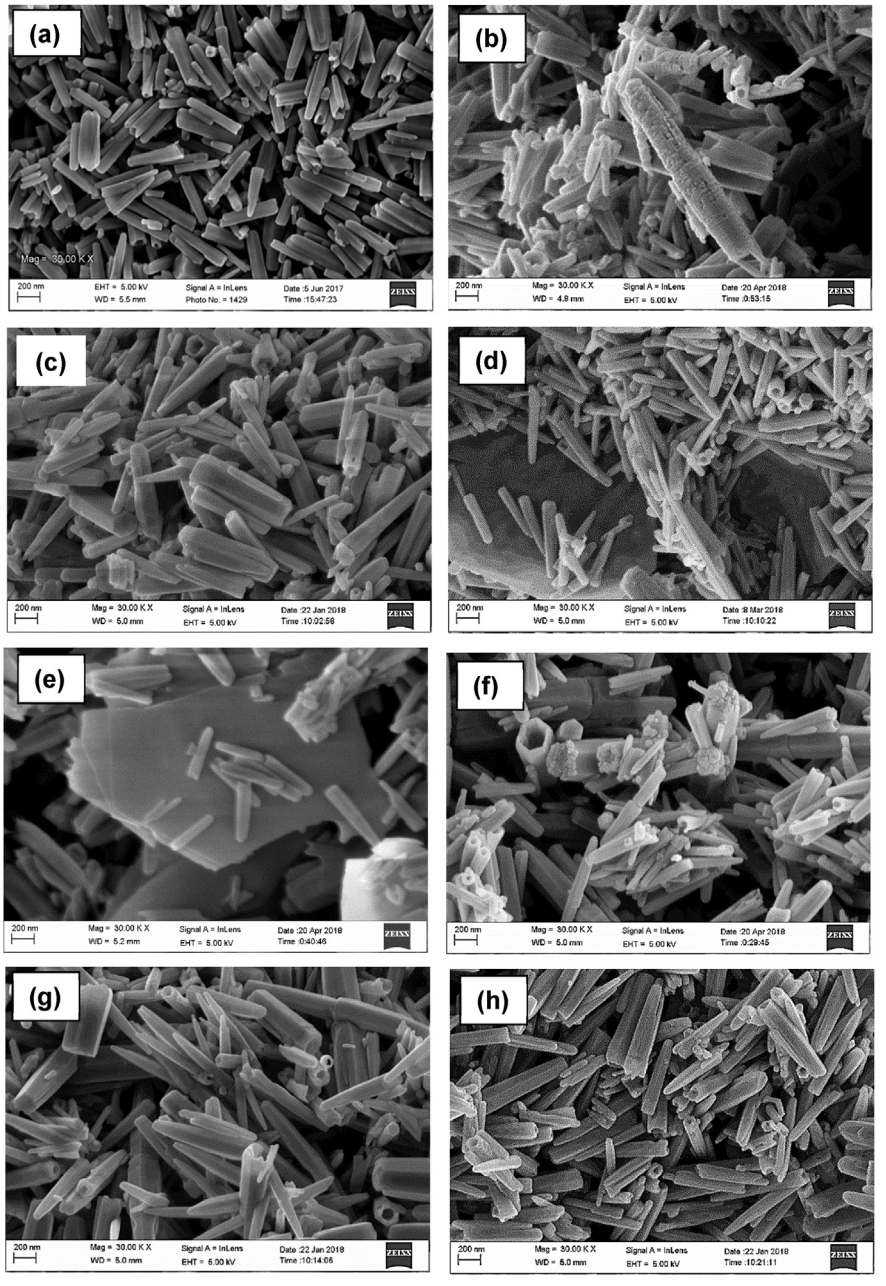

Fig. 10. SEM images of (a) ZnO, (b) Cu/ZnO, (c) Ag/ZnO, (d) Pb/ZnO, (e) Cr/ZnO, (f) Mn/ZnO, (g) Cd/ZnO and (h) Ni/ZnO hybrid particles after removal of heavy metal ions under visible light irradiation.

of ZnO particles. These tiny particles might be the evidence of the photo-reduction of Ag^{+} ions and would be analyzed further using EDX mapping. In contrary, plate-like precipitates were observed in Pb/ZnO hybrid particles (Fig. 11(c)). The average diameter and length of Pb/ZnO hybrid particles were 80.79 ± 9.91nm and 497.95 ± 9.04nm, respectively. As displayed in Fig. 11(d), the deposited particles were not obviously seen on the surface of Cr/ZnO hybrid particles. The average diameter

https://doi.org/10.1016/j.heliyon.2019.e01440

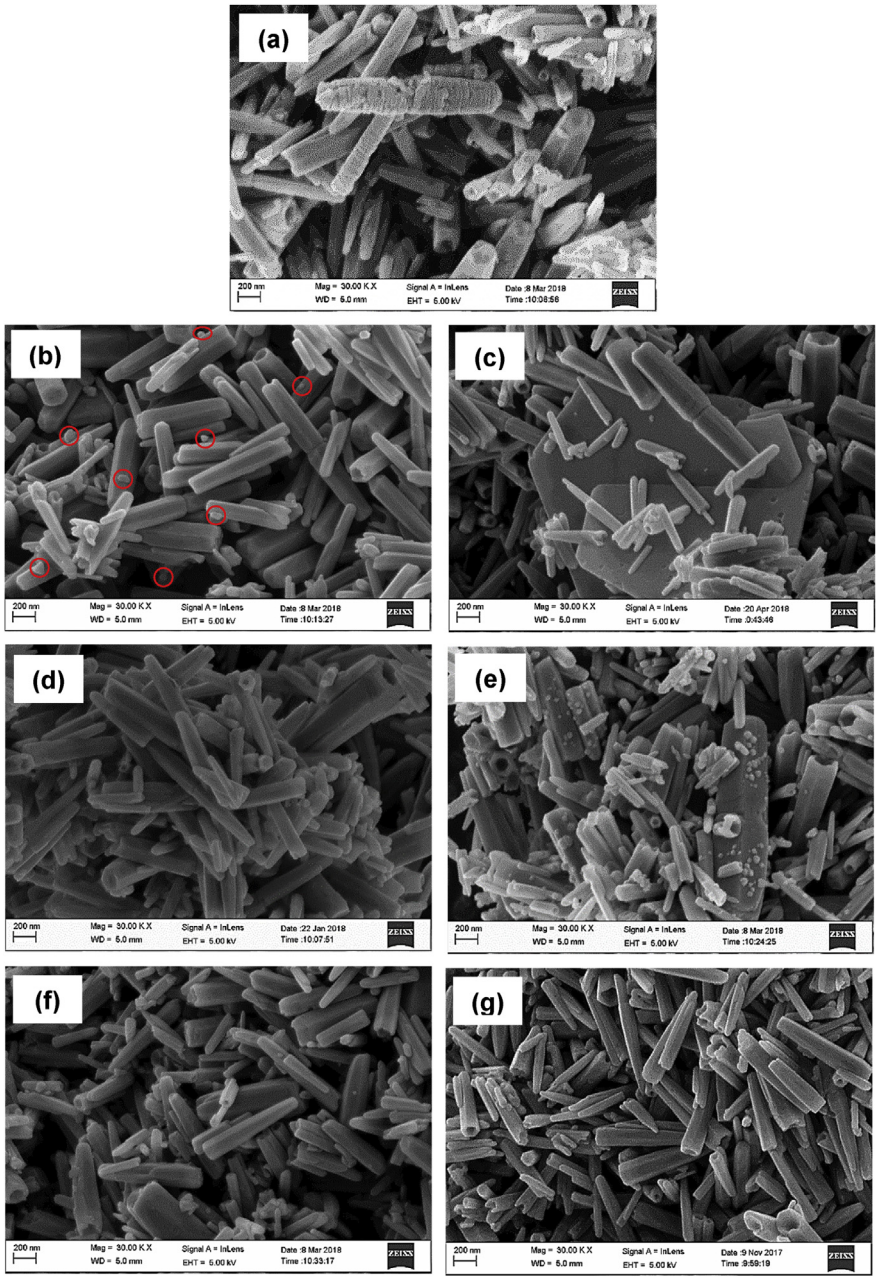

Fig. 11. SEM images of (a) Cu/ZnO, (b) Ag/ZnO, (c) Pb/ZnO, (d) Cr/ZnO, (e) Mn/ZnO, (f) Cd/ZnO and (g) Ni/ZnO hybrid particles after removal of heavy metal ions under UV light irradiation.

and length of Cr/ZnO hybrid particles were 99.36 ± 6.58nm and 594.01 ± 10.75nm, respectively. Fig. 11(e) clearly shows many particles deposited onto the surface of ZnO particles, which increased the size of ZnO particles. For instance, the average diameter and length of Mn/ZnO hybrid particles were 110.84 ± 10.98nm and 579.92 ± 17.31nm, respectively. Nevertheless, the deposition of Cd(II) and Ni(II) was not obviously seen on the SEM image of Fig. 11(f) and (g). The average diameter and length of Cd/ZnO hybrid particles were 105.58 ± 11.64nm and 547.09 ± 13.31nm,

https://doi.org/10.1016/j.heliyon.2019.e01440

respectively. Similarly, the average diameter and length of Ni/ZnO hybrid particles were 107.57 ± 18.57nm and 579.31 ± 14.35nm, respectively.

As shown in Fig. 1, the UV irradiation has a significant influence on the removal of heavy metal ions by ZnO particles as compared to visible light. Therefore, TEM analysis was used to analyze the structure of M/ZnO hybrid particles collected after UV irradiation process. The deposition of Cu(II) ions onto the surface of ZnO particles was clearly observed via TEM image as displayed in Fig. 12(a). The surface of Cu/ZnO hybrid particles was coated with a foreign layer. The HRTEM image in Fig. 12(b) shows that Cu-O layer was deposited onto the surface of ZnO particles with lattice fringes of 0.25nm, corresponding to the (002) plane of monoclinic CuO. The EDX mapping of Fig. 12(c)−(e) indicate the presence of high concentration of Cu element all over the surface of ZnO particles.

As shown in Fig. 13(a), Ag particles were clearly found on the surface of ZnO particles. The diameter of Ag particles was <25nm. The HRTEM image in Fig. 13(b) reveals that the lattice fringes of the ZnO and the Ag particles were 0.26nm and 0.23nm, respectively. These inter-planar distances correspond to the (002) plane of the wurtzite ZnO while the (111) plane of the cubic Ag phase. The EDX analysis in Fig. 13(c)−(e) verifies that Ag particles were deposited on the surface of ZnO particles. The results are consistent with the XRD and XPS findings.

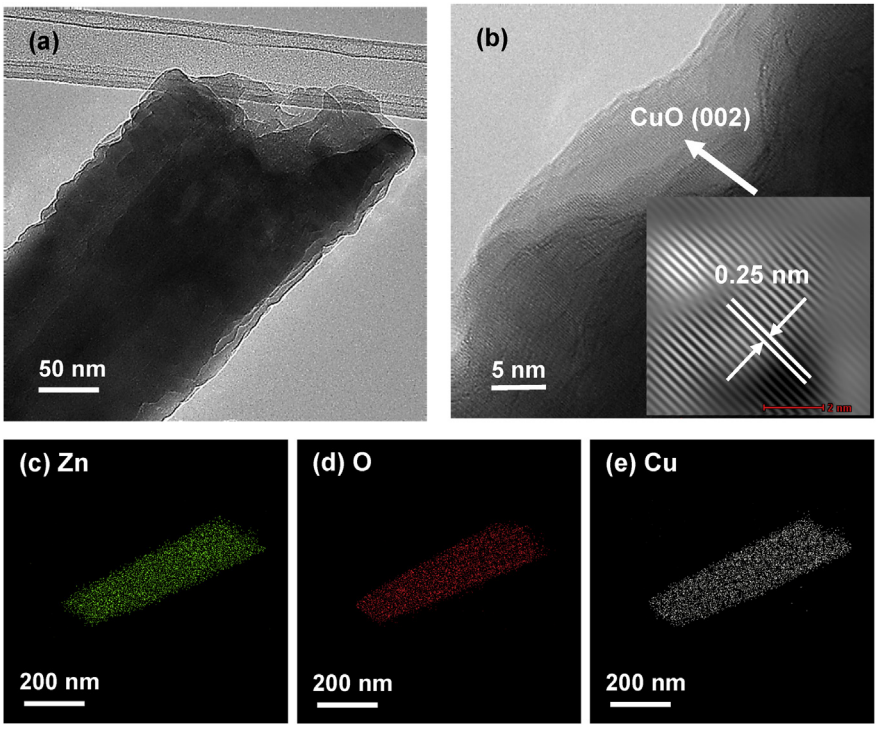

Fig. 12. (a) TEM images, (b) HRTEM image and EDX mapping of (c) Zn, (d) O and (e) Cu element of ZnO particles after the removal of Cu(II) under UV irradiation.

https://doi.org/10.1016/j.heliyon.2019.e01440

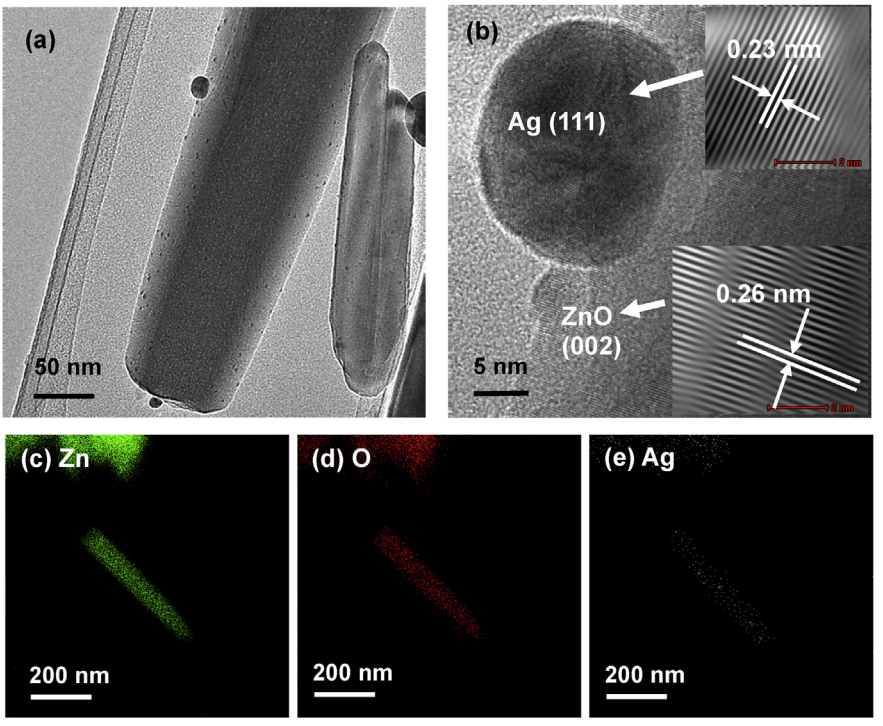

Fig. 13. (a) TEM images, (b) HRTEM image and EDX mapping of (c) Zn, (d) O and (e) Ag element of ZnO particles after the removal of Ag(I) under UV irradiation.

It is clear from Fig. 14(a) that plate-like structure was formed in Pb/ZnO hybrid particles. A closer examine in HRTEM reveals that the plate-like structure composed of $Pb(OH)_2$ and PbO_2 crystal grains as shown in Fig. 14(b). The 0.32nm was lattice spacing of (011) plane of $Pb(OH)_2$ whereas the lattice spacing of 0.28nm of (110) plane belongs to PbO_2. The formation of these plate-like structures indicates that nucleation and crystallization also occurred in the solution. Fig. 14(c)−(e) displays the EDX mapping analysis, indicating that plate-like structure contained high intensity of Pb and O.

The deposition of Cr particles was not obviously seen on the surface of ZnO particles under UV light as shown in Fig. 15(a), (b). From HRTEM image of Cr/ZnO hybrid particles, well-spaced lattice fringes indicated the high crystalline quality of ZnO particles. The lattice spacing was measured to be 0.26nm, corresponding to (002) plane of ZnO hexagonal. No other lattice fringe was found in the Cr/ZnO hybrid particles. The evidence of the reduction of Cr(VI) by ZnO particles catalyst was provided by EDX elemental mappings of the Cr/ZnO hybrid particles as shown in Fig. 15(c)−(e) which shown the distribution of Cr on the surface of ZnO particles after the removal process.

Fig. 16(a) displays the micrographs of Mn/ZnO hybrid particles, with many tiny particles deposited on its surface. In Fig. 16(b), HRTEM micrographs reveal the presence

https://doi.org/10.1016/j.heliyon.2019.e01440

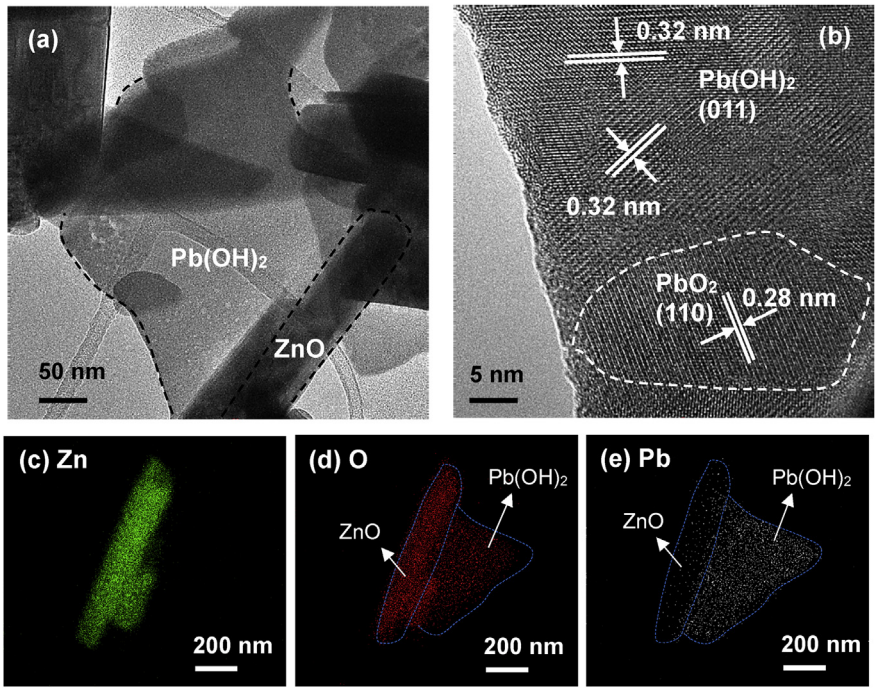

Fig. 14. (a) TEM images, (b) HRTEM image and EDX mapping of (c) Zn, (d) O and (e) Pb element of ZnO particles after the removal of Pb(II) under UV irradiation.

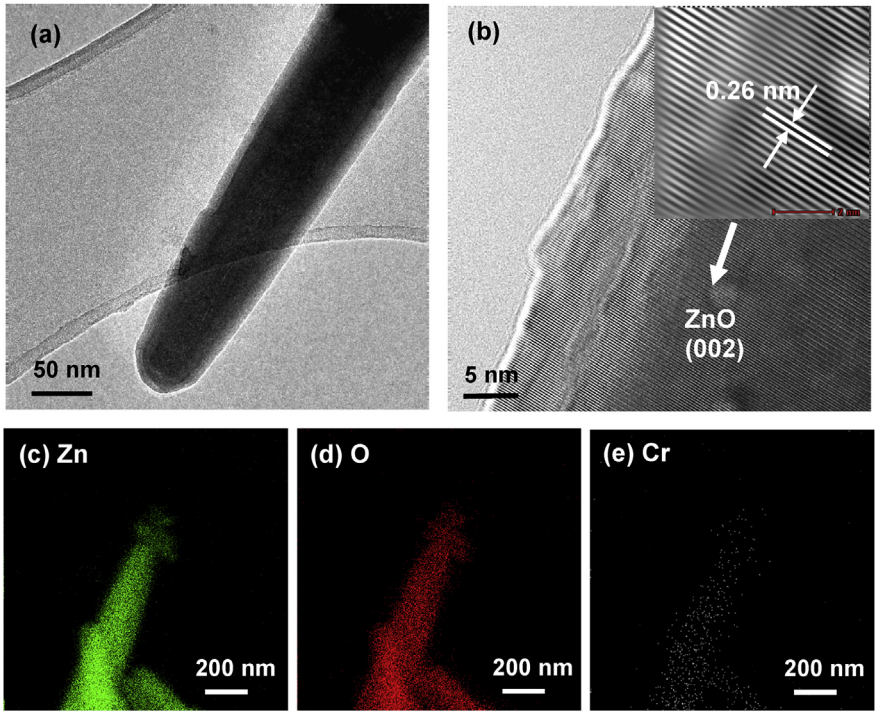

Fig. 15. (a) TEM images, (b) HRTEM image and EDX mapping of (c) Zn, (d) O and (e) Cr element of ZnO particles after the removal of Cr(VI) under UV irradiation.

https://doi.org/10.1016/j.heliyon.2019.e01440

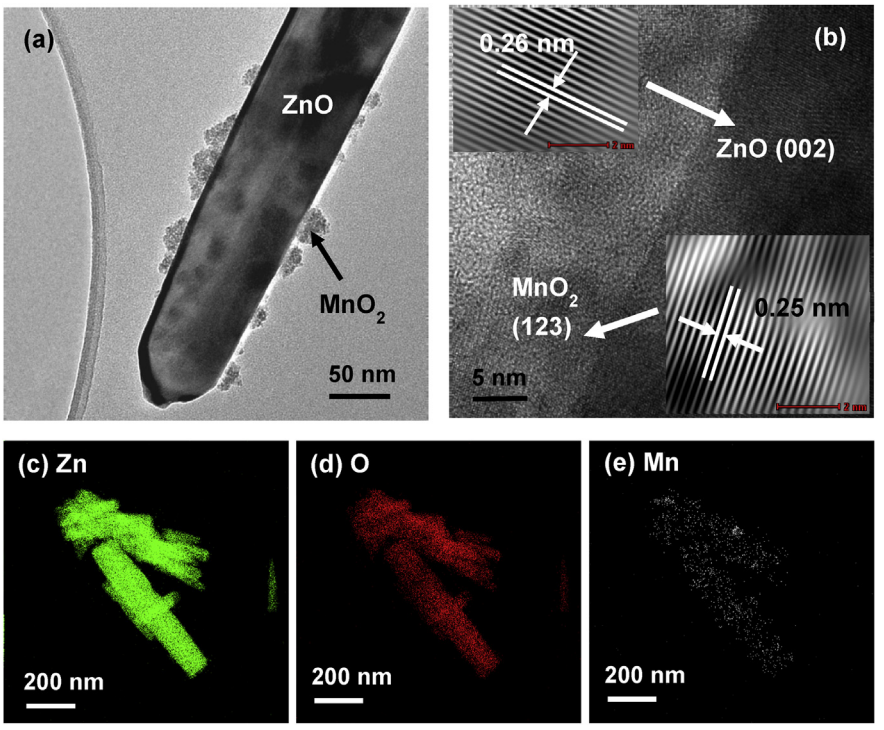

Fig. 16. (a) TEM images, (b) HRTEM image and EDX mapping of (c) Zn, (d) O and (e) Mn element of ZnO particles after the removal of Mn(II) under UV irradiation.

of the ZnO hexagonal phase identified by the spacing d = 0.26nm and indexed as (002) plane. The tiny particles of MnO_2 cubic phase were found with lattice spacing d = 0.25nm and indexed as (123) plane. The distribution of Mn element on ZnO particles was further confirmed by EDX mapping analysis as shown in Fig. 16(c)−(e).

However, the removal of Cd(II) and Ni(II) under UV radiation was not obviously seen via the TEM morphology analysis which displayed in Figs. 17(a) and 18(a), respectively. The HRTEM images of both Cd/ZnO and Ni/ZnO hybrid particles belong to the hexagonal phase of ZnO, which is also identified by the spacing d = 0.26nm and indexed as (002) plane (see Figs. 17(b) and 18(b). The presence of Cd or Ni on ZnO particles was detected by the EDX mapping in Figs. 17(c)−(e) and 18(c)−(e), respectively. The amount of Cd or Ni element was not significant as compared to Zn and O element. The types of deposits found on the surface of ZnO particles via XRD, XPS, SEM, TEM, HRTEM and EDX mapping are summarized in Table 2.

3.3. Heavy metal ions removal mechanisms by ZnO particles

Base on the evidences collected in Table 2, two types of heavy metal ions removal mechanisms by ZnO particles are proposed, i.e. (i) physical adsorption and (ii) reduction/oxidation by photo-generated electron-hole pairs.

https://doi.org/10.1016/j.heliyon.2019.e01440

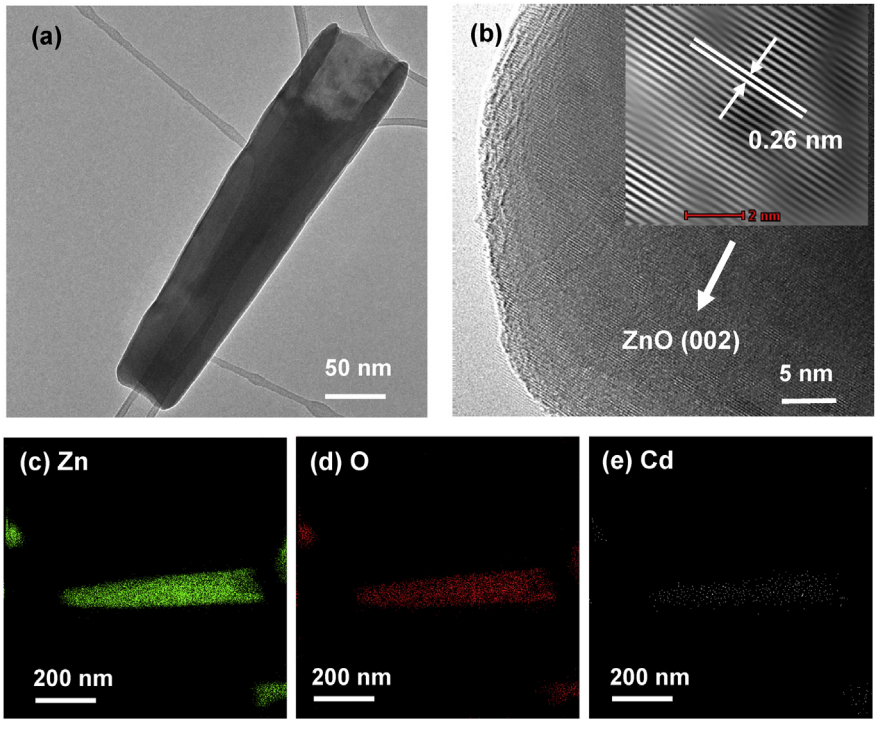

Fig. 17. (a)TEM images, (b) HRTEM image and EDX mapping of (c) Zn, (d) O and (e) Cd element of ZnO particles after the removal of Cd(II) under UV irradiation.

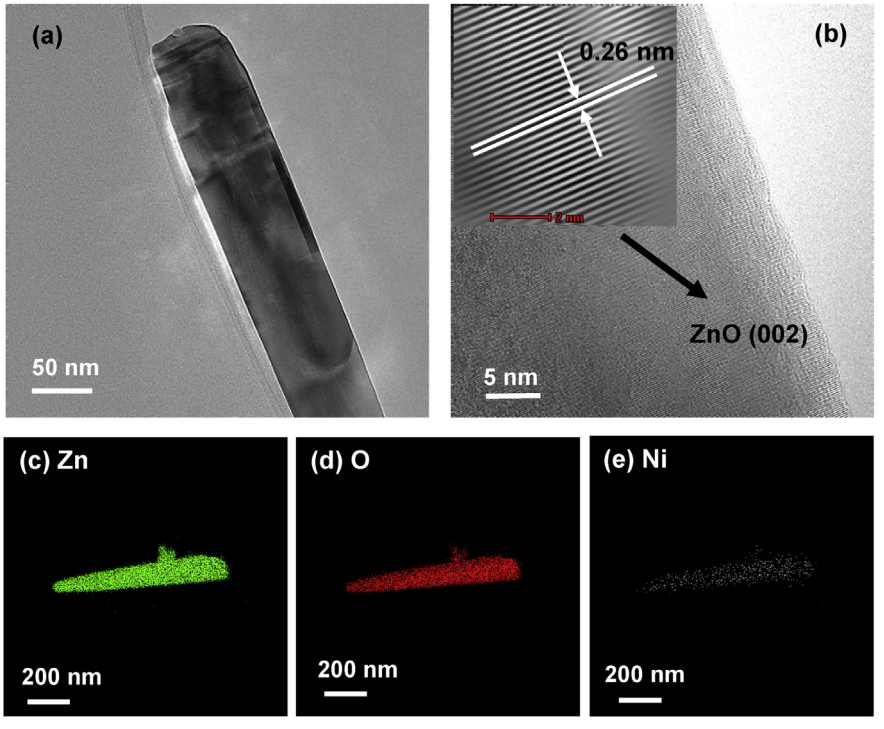

Fig. 18. (a) TEM images, (b) HRTEM image and EDX mapping of (c) Zn, (d) O and (e) Ni element of ZnO particles after the removal of Ni(II) under UV irradiation.

https://doi.org/10.1016/j.heliyon.2019.e01440

Table 2. Deposition of metal/metal oxide onto the surface of ZnO particles under UV irradiation and their removal mechanisms.

Hybrid particles	XPS	XRD		SEM		TEM	HRTEM	EDX mapping	Types of deposits	Dominant removal mechanism
	UV	UV	Visible	UV	Visible	UV				
Ag/ZnO	Ag	Ag	-	Particles	-	Particles	Ag particles	Ag	Ag particles	Reduction
Cr/ZnO	Cr_2O_3	-	Cr_2O_3	-	Flake-like	-	-	Cr	Cr_2O_3 particles	Reduction
Pb/ZnO	PbO_2 $Pb(OH)_2$	$Pb(OH)_2$ PbO_2	$Pb(OH)_2$	Flake- like	Flake- like	Flake-like	$Pb(OH)_2$ PbO_2	Pb, O	$Pb(OH)_2 + PbO_2$ flakes	Oxidation
Mn/ZnO	-	MnO_2	-	Particles	Particles	Particles	MnO_2	Mn, O	MnO_2 particles	Oxidation
Cu/ZnO	CuO Cu_2O	CuO	CuO	Rough surface	Rough surface	Thin film	CuO thin film	Cu, O	CuO thin film Cu_2O	Adsorption Reduction
Cd/ZnO	-	-		-		-	-	Cd	Cd thin film (if any)	Adsorption
Ni/ZnO	-	-		-		-	-	Ni	Ni thin film (if any)	Adsorption

https://doi.org/10.1016/j.heliyon.2019.e01440

(i) Physical adsorption

As measured by zeta potential analyzer, ZnO particles were negatively charged with value of -23.6mV as shown in Fig. 19. The negatively charged surface of ZnO particles was mainly contributed by the OH^- groups during the growth process as discussed by Thein et al. [11]. These OH^- groups became the actively adsorptive sites. As depicted in Fig. 20(a), the cationic of heavy metal in the aqueous solution tended to react with OH^- groups to form a thin film on the surface of ZnO particles. Similar observation was also reported by Wang et al. [34]. As the adsorption process was limited by the number of negative adsorptive sites on the surface of ZnO particles, the adsorption efficiency was usually poor and might reach a saturation level after a period of time. As the optical energy of visible light was insufficient to cause ZnO particles generate electrons and holes, thus the removal of metal ions from solution by ZnO particles was via physical adsorption process. In addition, the removal of Cd(II) ions and Ni(II) ions by ZnO particles under UV light was also categorized in this mechanism as no obvious change was observed in their removal efficiency.

(ii) Reduction/oxidation by photogenerated electron-hole pairs

The reduction happened when the redox potential of metal is more positive than the e^-_{CB} level of ZnO particles. Theoretically, metal ions that expected to experience reduction are Ag(I) ions, Cr(VI) ions and Cu(II) ions. The oxidation of metal ions is selectively occurred when oxidation potential is less positive than the h^+_{VB} level [10]. According to the results, oxidation occurred at Pb(II) and Mn(II) ions. It is worth mentioning that as long as the appropriate optical excitation source is available, many electrons and holes could be generated continuously for the reduction or oxidation of metal ions as illustrated in Fig. 20(b). Thus, the metal/metal oxides could present in the form of thin film on the surface of ZnO particles or as particles that either deposited onto the surface of ZnO particles or in the solution.

In brief, the heavy metal ions were removed by ZnO particles either by one of the above-mentioned mechanisms or combined mechanisms depend on the types of

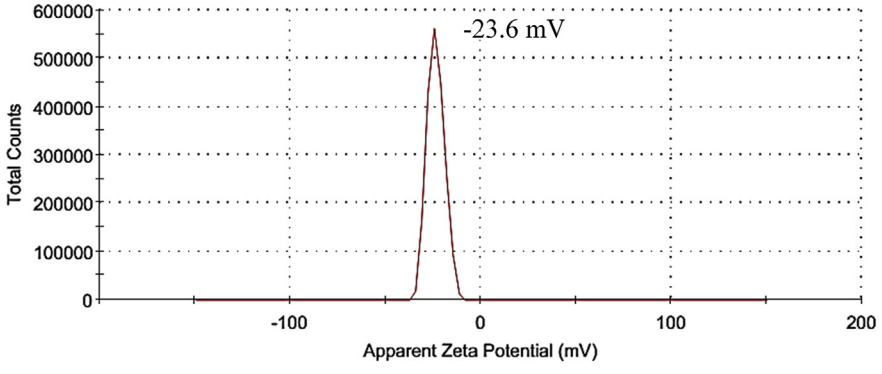

Fig. 19. Surface charge of ZnO particles measured by zeta potential.

https://doi.org/10.1016/j.heliyon.2019.e01440

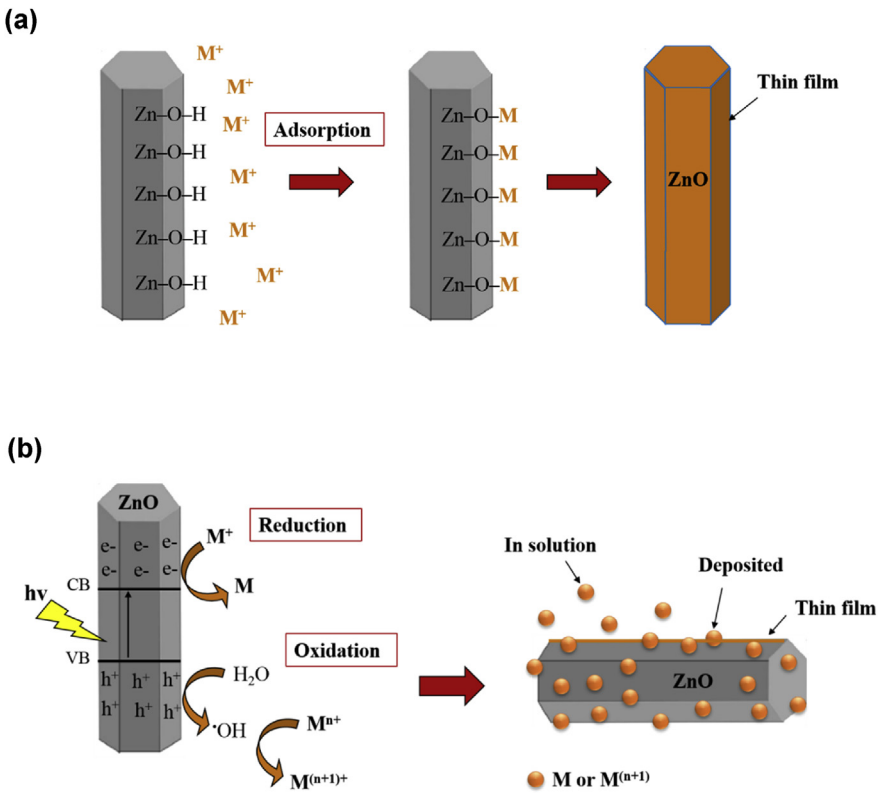

Fig. 20. Mechanisms of heavy metal ions removal using ZnO particles via (a) adsorption and (b) reduction/oxidation process.

metal ions and types of light sources. For instance, the Cu(II) ions were completely removed within 15min under visible illumination as shown in Fig. 1(a). The formation of thick CuO layer on the surface of ZnO particles suggests that the Cu(II) ions were hydrated and formed $Cu(H_2O)_6^{2+}$ ions. These ions were further reacted with OH^- ions via a Lewis interaction, leading to the formation of CuO layer via absorption [34]. The removal of Cu(II) ions by ZnO particles photocatalyst under UV light irradiation was possible via reduction due to its reduction potential of Cu^{2+}/Cu^+ was +0.15V [35].

In the visible irradiation, the photoreduction of Ag(I) was unlikely occurred as the excited energy was not strong enough to generate electrons from ZnO catalyst. Thus, in such condition, the slight removal of Ag(I) was supposed due to the absorption of Ag^+ ions onto the ZnO surface. The negative charged active sites of ZnO particles attracted the Ag^+ cations, leading to the slight removal of Ag^+ ions from solution. In contrary, the removal of Ag(I) ions using ZnO particles under UV irradiation were caused by photocatalytic reduction. As highlighted in Eq. (2), the redox potential of Ag^+/Ag^0 is more positive than the energy level of e^-_{CB} of ZnO [10, 36, 37]. Therefore, electrons were generated by ZnO particles during optical excitation Eq. (3). These electrons were captured by Ag(I) ions, causing metal deposition onto

https://doi.org/10.1016/j.heliyon.2019.e01440

the surface of ZnO particles. As a consequence, a significant removal of Ag(I) ions was observed as shown in Fig. 1(c).

$$Ag^{+} + e^{-} \rightarrow Ag^{0} \ (E^{o} = +\ 0.79V) \quad (2)$$

$$ZnO + h\nu \rightarrow h^{+} + e^{-} \quad (3)$$

As shown in Fig. 1, ZnO particles demonstrated moderate removal efficiency of Pb(II) ions under visible light but excellent performance under UV light illumination. The removal of Pb(II) ions from solution under visible light condition were caused by the formation of flake-like particles. The Pb(II) ions reacted with OH^{-} ions to form $Pb(OH)_2$ crystals. With the exposure of UV light, the removal of Pb(II) ions was improved via photo-oxidation of Pb(II) ions. The Pb(II) ions could also be oxidized by capturing holes or $^{\bullet}OH$ radicals present in the solution and reacted with the dissolved O^{2-} ions to form PbO_2 as expressed by Eq. (4) [8].

$$Pb^{2+} \rightarrow Pb^{4+} + 2e^{-} \ (E^{0} = -\ 0.67V) \quad (4)$$

The behavior of Cr(VI) ions removal under visible light irradiation was opposed to Ag(I) ions. The removal efficiency of Cr(VI) under visible light was much higher than that of UV light process. Beside the adsorption of Cr(VI) ions on the negatively charged surface of ZnO particles, the removal of Cr(VI) ions was also enhanced by the formation of Cr_2O_3 plate-like precipitates as displayed in Fig. 11(c). On the contrary, the removal efficiency of Cr(VI) ions by ZnO particles was suppressed under UV light. In theory, the reduction of Cr(VI) ions to Cr(III) ions by photogenerated electrons from ZnO particles under UV irradiation was possible [8]. Thus, some of the Cr(VI) ions was reduced to Cr(III) ions. Nevertheless, both Cr(VI) ions and Cr(III) ions were still present in the solution. Therefore, the total numbers of Cr ions in the solution only decrease slightly as measured by ICP-OES. Small amount of the Cr(VI) ions were adsorbed on the surface of ZnO particles as Cr thin film.

Under visible light irradiation, the removal of Mn(II) ions from solution was attributed to the physical absorption of cationic Mn^{2+} onto the negatively charged surface of ZnO particles. The removal efficiency of Mn(II) ions improved slightly under UV irradiation. It is known that the Mn(II) ions were not able to reduce by the photocatalytic reaction of ZnO under UV irradiation. This is because the reduction potential standard of Mn^{2+}/Mn ($E^{0} = -1.18V$ vs. NHE) is more negative than the e^{-}_{CB} level of ZnO particles [38]. Therefore, the oxidative route seems to be the preferred photocatalytic pathway in the presence of ZnO particles under UV irradiation. The Mn(II) ions were oxidized by holes which generated by ZnO during the absorption of photons. The oxidation potential of Mn^{2+} to Mn^{4+} equal to 1.22V vs. NHE [35] as shown in Eq. (5). Subsequently, the Mn^{4+} ions reacted with dissolved oxygen to

https://doi.org/10.1016/j.heliyon.2019.e01440

form MnO_2 particles, as observed in Fig. 15(a). The poor removal efficiency of Mn(II) ions in the photocatalytic process of ZnO indicates that the oxidation reaction took place slowly.

$$Mn^{2+} + h^{+}_{VB} \rightarrow Mn^{4+} \ (E^0 = 1.22V) \quad (5)$$

The poor removal of Cd(II) or Ni(II) ions by ZnO particles were recorded under UV and visible light irradiation. The UV radiation did not cause significant effect on the removal of Cd(II) or Ni(II) ions as compared to other ions. The negative standard reduction potential of Ni^{2+}/Ni and Cd^{2+}/Cd were - 0.43V and - 0.25V, respectively [39, 40]. As a consequence, the photochemical reduction of Cd(II) or Ni(II) ions were not able to occur. The slight removal of Cd(II) or Ni(II) ions (<7.2%) could be due to the adsorption of Cd^{2+} or Ni^{2+} ions onto the negative sites of ZnO surface [41].

4. Conclusions

ZnO particles demonstrated its remarkable ability to remove heavy metal ions such as Cu(II), Ag(I), Pb(II) and Cr(VI) but poor removal efficiencies on Mn(II), Cd(II) and Ni(II) ions under UV light. The ZnO particles removed Cu(II), Cr(VI) and Ag(I) ions by reduction; Pb(II) and Mn(II) ions by oxidation whereas Cd(II) and Ni(II) ions by adsorption under UV irradiation. In contrary, the removal of these metal ions were by adsorption under visible light irradiation. Thus, the removal mechanisms of heavy metal ions by ZnO particles depended on the types of metal ions and light source rather than the common accepted reduction mechanism. This study suggests that ZnO particles shall use in wastewater containing Cu(II), Ag(I), Pb(II) and Cr(VI) ions for effective removal of these heavy metal ions. Also, the selective nature of heavy metal ions removal under different light sources by ZnO could be used to develop ZnO based heavy metal ions sensor.

Declarations

Author contribution statement

Anh T. Le: Conceived and designed the experiments; Performed the experiments; Analyzed and interpreted the data; Contributed reagents, materials, analysis tools or data; Wrote the paper.

Swee-Yong Pung: Conceived and designed the experiments; Analyzed and interpreted the data; Contributed reagents, materials, analysis tools or data; Wrote the paper.

Srimala Sreekantan, Atsunori Matsuda, Dai P. Huynh: Analyzed and interpreted the data.

https://doi.org/10.1016/j.heliyon.2019.e01440

Funding statement

This work was supported by Universiti Sains Malaysia (Briding Grant) (1001.PBAHAN.8014095) and AUN/SEED Net under Collaborative Research Program (CR) (304.PBAHAN.6050354).

Competing interest statement

The authors declare no conflict of interest.

Additional information

No additional information is available for this paper.

References

[1] M. Al-Shannag, Z. Al-Qodah, K. Bani-Melhem, M.R. Qtaishat, M. Alkasrawi, Heavy metal ions removal from metal plating wastewater using electrocoagulation: kinetic study and process performance, Chem. Eng. J. 260 (2015) 749–756.

[2] E. Brillas, C.A. Martínez-Huitle, Decontamination of wastewaters containing synthetic organic dyes by electrochemical methods. An updated review, Appl. Catal. B Environ. 166 (2015) 603–643.

[3] R.S. Hebbar, A.M. Isloor, K. Ananda, A. Ismail, Fabrication of polydopamine functionalized halloysite nanotube/polyetherimide membranes for heavy metal removal, J. Mater. Chem. 4 (2016) 764–774.

[4] M.R.S. Kebria, M. Jahanshahi, A. Rahimpour, SiO_2 modified polyethyleneimine-based nanofiltration membranes for dye removal from aqueous and organic solutions, Desalination 367 (2015) 255–264.

[5] T. Zewail, N. Yousef, Kinetic study of heavy metal ions removal by ion exchange in batch conical air spouted bed, Alexandria Eng J 54 (2015) 83–90.

[6] A. Abbas, A.M. Al-Amer, T. Laoui, M.J. Al-Marri, M.S. Nasser, M. Khraisheh, M.A. Atieh, Heavy metal removal from aqueous solution by advanced carbon nanotubes: critical review of adsorption applications, Separ. Purif. Technol. 157 (2016) 141–161.

[7] J.-G. Yu, X.-H. Zhao, H. Yang, X.-H. Chen, Q. Yang, L.-Y. Yu, J.-H. Jiang, X.-Q. Chen, Aqueous adsorption and removal of organic contaminants by carbon nanotubes, Sci. Total Environ. 482 (2014) 241–251.

https://doi.org/10.1016/j.heliyon.2019.e01440

[8] E. Wahyuni, N. Aprilita, H. Hatimah, A. Wulandari, M. Mudasir, Removal of toxic metal ions in water by photocatalytic method, Am. Chem. Sci. J. 5 (2015) 194–201.

[9] H.M. Yadav, J.-S. Kim, S.H. Pawar, Developments in photocatalytic antibacterial activity of nano TiO_2: a review, Kor. J. Chem. Eng. 33 (2016) 1989–1998.

[10] M.I. Litter, Mechanisms of removal of heavy metals and arsenic from water by TiO_2-heterogeneous photocatalysis, Pure Appl. Chem. 87 (2015) 557–567.

[11] M.T. Thein, S.-Y. Pung, A. Aziz, M. Itoh, Stacked ZnO nanorods synthesized by solution precipitation method and their photocatalytic activity study, J. Sol. Gel Sci. Technol. 74 (2015) 260–271.

[12] C.B. Ong, L.Y. Ng, A.W. Mohammad, A review of ZnO nanoparticles as solar photocatalysts: synthesis, mechanisms and applications, Renew. Sustain. Energy Rev. 81 (2018) 536–551.

[13] X. Chen, Z. Wu, D. Liu, Z. Gao, Preparation of ZnO photocatalyst for the efficient and rapid photocatalytic degradation of Azo dyes, Nanoscale Res Lett 12 (2017) 143.

[14] S. Singh, K. Barick, D. Bahadur, Novel and efficient three dimensional mesoporous ZnO nanoassemblies for envirnomental remediation, Int. J. Nanosci. 10 (2011) 1001–1005.

[15] F. Fu, Q. Wang, Removal of heavy metal ions from wastewaters: a review, J. Environ. Manag. 92 (2011) 407–418.

[16] X. Wang, W. Cai, S. Liu, G. Wang, Z. Wu, H. Zhao, ZnO hollow microspheres with exposed porous nanosheets surface: structurally enhanced adsorption towards heavy metal ions, Colloids Surf., A 422 (2013) 199–205.

[17] M. Qamar, M. Gondal, Z. Yamani, Laser-induced efficient reduction of Cr (VI) catalyzed by ZnO nanoparticles, J. Hazard Mater. 187 (2011) 258–263.

[18] K. Joshi, V. Shrivastava, Photocatalytic degradation of Chromium (VI) from wastewater using nanomaterials like TiO_2, ZnO, and CdS, Appl. Nanosci. 1 (2011) 147–155.

[19] S. Chakrabarti, B. Chaudhuri, S. Bhattacharjee, A.K. Ray, B.K. Dutta, Photoreduction of hexavalent chromium in aqueous solution in the presence of zinc oxide as semiconductor catalyst, Chem. Eng. J. 153 (2009) 86–93.

[20] A. Assadi, M.H. Dehghani, N. Rastkari, S. Nasseri, A.H. Mahvi, Photocatalytic reduction of hexavalent chromium in aqueous solutions with zinc oxide nanoparticles and hydrogen peroxide, Environ. Protect. Eng. 38 (2012) 5–16.

https://doi.org/10.1016/j.heliyon.2019.e01440

[21] M. Shirzad-Siboni, M. Farrokhi, R. Darvishi Cheshmeh Soltani, A. Khataee, S. Tajassosi, Photocatalytic reduction of hexavalent chromium over ZnO nanorods immobilized on kaolin, Ind. Eng. Chem. Res. 53 (2014) 1079−1087.

[22] J. Liu, Y. Zhao, J. Ma, Y. Dai, J. Li, J. Zhang, Flower-like ZnO hollow microspheres on ceramic mesh substrate for photocatalytic reduction of Cr (VI) in tannery wastewater, Ceram. Int. 42 (2016) 15968−15974.

[23] M. Shirzad Siboni, M. Samadi, J. Yang, S. Lee, Photocatalytic reduction of Cr (VI) and Ni (II) in aqueous solution by synthesized nanoparticle ZnO under ultraviolet light irradiation: a kinetic study, Environ. Technol. 32 (2011) 1573−1579.

[24] J.C. Lee, H.-S. Kim, J.-H. Lee, S. Park, Photocatalytic removal of Cu ions from aqueous Cu-EDTA solution using solution combusted zinc oxide nanopowder, J. Nanosci. Nanotechnol. 8 (2008) 5284−5287.

[25] J.H. Lee, J.U. Seo, Y.J. Chung, J.C. Lee, S. Park, Removal of heavy metal ions from aqueous Pb-EDTA and Cu-EDTA solutions using nanosized ZnO powders by solution-combustion method, Key Eng. Mater. (2006) 837−840.

[26] J. Preethi, M.H. Farzana, S. Meenakshi, Photo-reduction of Cr (VI) using chitosan supported zinc oxide materials, Int. J. Biol. Macromol. 104 (2017) 1783−1793.

[27] L. Zhu, M. Hong, G.W. Ho, Fabrication of wheat grain textured TiO_2/CuO composite nanofibers for enhanced solar H_2 generation and degradation performance, Nano Energy 11 (2015) 28−37.

[28] K. Munawar, M.A. Mansoor, W.J. Basirun, M. Misran, N.M. Huang, M. Mazhar, Single step fabrication of CuO−MnO−2TiO_2 composite thin films with improved photoelectrochemical response, RSC Adv. 7 (2017) 15885−15893.

[29] S. Singh, R. Singhal, V.S. Kumar, Study on swift heavy ions induced modifications of Ag-ZnO nanocomposite thin film, Superlattice. Microst. 103 (2017) 195−204.

[30] W.-H. Yang, H.-H. Wang, D.-H. Chen, Z.-Y. Zhou, S.-G. Sun, Facile synthesis of a platinum−lead oxide nanocomposite catalyst with high activity and durability for ethanol electrooxidation, Phys. Chem. Chem. Phys. 14 (2012) 16424−16432.

[31] J. Morales, G. Petkova, M. Cruz, A. Caballero, Nanostructured lead dioxide thin electrode, Electrochem Solid St. 7 (2004) A75−A77.

https://doi.org/10.1016/j.heliyon.2019.e01440

[32] T. Zhou, C. Li, H. Jin, Y. Lian, W. Han, Effective adsorption/reduction of Cr (VI) oxyanion by halloysite@ polyaniline hybrid nanotubes, ACS Appl Mater Inter 9 (2017) 6030−6043.

[33] R.R. Salunkhe, H. Ahn, J.H. Kim, Y. Yamauchi, Rational design of coaxial structured carbon nanotube−manganese oxide (CNT−MnO_2) for energy storage application, Nanotechnology 26 (2015) 204004.

[34] X. Wang, W. Cai, Y. Lin, G. Wang, C. Liang, Mass production of micro/nanostructured porous ZnO plates and their strong structurally enhanced and selective adsorption performance for environmental remediation, J. Mater. Chem. 20 (2010) 8582−8590.

[35] AllenJ. Bard, Roger Parson, Joseph Jordan, Standard Potentials in Aqueous Solution, 2017.

[36] W. Wu, C. Jiang, V.A. Roy, Recent progress in magnetic iron oxide−semiconductor composite nanomaterials as promising photocatalysts, Nanoscale 7 (2015) 38−58.

[37] E. Albiter, M. Valenzuela, S. Alfaro, G. Valverde-Aguilar, F. Martínez-Pallares, Photocatalytic deposition of Ag nanoparticles on TiO_2: metal precursor effect on the structural and photoactivity properties, J Saudi Chem Soc 19 (2015) 563−573.

[38] M.I. Litter, Treatment of chromium, mercury, lead, uranium, and arsenic in water by heterogeneous photocatalysis, Adv. Chem. Eng. 36 (2009) 37−67.

[39] I.A. Ruvarac-Bugarčić, Z.V. Šaponjić, S. Zec, T. Rajh, J.M. Nedeljković, Photocatalytic reduction of cadmium on TiO_2 nanoparticles modified with amino acids, Chem. Phys. Lett. 407 (2005) 110−113.

[40] C. Chenthamarakshan, K. Rajeshwar, E.J. Wolfrum, Heterogeneous photocatalytic reduction of Cr(VI) in UV-irradiated titania suspensions: effect of protons, ammonium ions, and other interfacial aspects, Langmuir 16 (2000) 2715−2721.

[41] V. Quaranta, M. Hellström, J. r. Behler, Proton-transfer mechanisms at the water−ZnO interface: the role of presolvation, J. Phys. Chem. Lett. 8 (2017) 1476−1483.

https://doi.org/10.1016/j.heliyon.2019.e01440